Photochemical and Magnetic Resonance Investigations of the Supramolecular Structure and Dynamics of Molecules and Reactive Radicals on the External and Internal Surface of MFI Zeolites§

Nicholas J. Turro,*,† Xue-Gong Lei,† Wei Li,†,‡ Zhiqiang Liu,† Ann McDermott,† M. Francesca Ottaviani,|| and Lloyd Abrams⊥

Contribution from the Department of Chemistry, Columbia University, New York, New York 10027, Institute of Chemical Sciences, University of Urbino, 61029 Urbino, Italy, and Central Research and Development Department, E. I. DuPont de Nemours and Co., Inc., Wilmington, Delaware 19880

Received May 17, 2000. Revised Manuscript Received September 26, 2000

Abstract: Photochemical, magnetic resonance, adsorption isotherms, and surface area measurements have been integrated to investigate the surface coverage dependence of the supramolecular structure and dynamics of two isomeric ketones, oMeDBK (molecular cross section similar to that of *o*-xylene) and pMeDBK (molecular cross section similar to that of *p*-xylene), adsorbed on three forms of zeolites with the MFI structure:silicalite, ZSM-5, and LZ-105. For each zeolite, the two isomeric ketones display striking qualitative differences in the experimental responses as a function of surface coverage. These differences are assigned to coverage-dependent changes in the supramolecular structural, dynamic, and binding characteristics of the adsorbed ketones and of the adsorbed reactive intermediates produced by photolysis of the ketones. In the case of pMeDBK, this ketone is adsorbed into the cages and channels of the internal surface. The external surface consists of two sites for the binding of oMeDBK: pores or "holes", and framework surface between the holes. The coverage dependence of the measured parameters for oMeDBK is consistent with a two-site model for adsorption on the external surface. Furthermore, a Langmuir expression for the adsorption isotherm of oMeDBK fits the experimental data for two binding sites. The entire array of data for oMeDBK is consistent with this model when the data are normalized for the different surface areas of the zeolites. Persistent radicals produced by the photolysis of oMeDBK and pMeDBK are observed directly by EPR analysis.

Introduction

Zeolites are versatile porous crystalline solids of industrial importance in the catalytic and in the separation sciences.[1−3] We report a supramolecular (guest@host) approach to the molecular level understanding of the catalytic and separation selectivity characteristics of zeolites. The guests serve as molecular probes of the host zeolitic structure. The latter controls the initial siting of the guests, the sieving probabilities, the size/shape selective diffusional dynamics, and the topology of diffusional pathways available to the adsorbed guests and to the reactive intermediates produced by photolysis of the adsorbed guest ketone molecules, oMeDBK and pMeDBK (Chart 1).

The photochemistry[4] of DBKs is well established in many supramolecular systems and can be employed to produce, at ambient temperatures, reactive radical intermediates at specific initial sites (in lieu of the production of reactive intermediates by adsorption on catalytic active acidic sites at elevated temperatures) on the external and internal surface of zeolites. Through the use of photochemical production of reactive intermediates and the elimination of effects due to chemically active acidic sites, *it is possible to decouple siting, diffusional, and sieving effects based on size and shape supramolecular features of guest@zeolite systems from the effects of active site acidity*. In this way the chemical aspects of zeolite catalysis can be separated from the physical binding and dynamic diffusional aspects, and the latter can be investigated separately.

Host Structure of MFI Zeolites. "Classical" zeolites[1] are *crystalline* inorganic polymers consisting of corner sharing AlO_4 and SiO_4 tetrahedra (Al and/or Si atoms connected through oxygen atoms) that make up the zeolite framework. The crystal structure of silicalite[5] serves as a model (Chart 1) for the MFI family of zeolites. In the ZSM-5 and LZ-105 samples employed

§ Contribution No. 8072.

† Columbia University.

‡ Present address: Department of Pharmaceutical Science, University of Tennessee, Memphis, TN 38163.

|| University of Urbino.

⊥ E. I. DuPont de Nemours and Co., Inc.

(1) (a) Csicsery, S. M. *Zeolite Chemistry & Catalysis*; Rabo, J. A., Ed.; ACS Monograph No. 171; American Chemical Society: Washington, DC, 1976; Chapter 12. (b) Derouane, E. G. *Zeolites: Science & Technology*; Ribeiro, F. R., Ed.; Nijhoff: Boston, 1984; p 347. (c) Derouane, E. G.; Gabelica, Z. *J. Catal.* **1980**, *65*, 486. (d) Derouane, E. G., Ed. *Diffusion and Shape Selective Catalysis in Zeolites*; Academic Press: New York, 1982.

(2) (a) Weisz, P. B. *Pure Appl. Chem.* **1980**, *52*, 2091. (b) Weisz, P. B. *Ind. Eng. Chem. Fundam.* **1986**, *25*, 53.

(3) (a) Lehn, J. M. *Supramolecular Chemistry*; VCH: New York, 1995. (b) Weiss, R. G.; Ramamurthy, V.; Hammond, G. S. *Acc. Chem. Res.* **1993**, *26*, 530. (c) Ramamurthy, V.; Weiss, R. G.; Hammond, G. S. *Adv. Photochem.* **1993**, *18*, 69.

(4) Photochemistry of dibenzyl ketone: (a) Engel, P. S. *J. Am. Chem. Soc.* **1970**, *92*, 6074−6076. (b) Robbins, W. K.; Eastman, R. H. *J. Am. Chem. Soc.* **1970**, *92*, 6076−6077. (c) Robbins, W. K.; Eastman, R. H. *J. Am. Chem. Soc.* **1970**, *92*, 6077−6079.

(5) (a) Flanigen, E. M.; Bennett, J. M.; Grose, R. W.; Cohen, J. P.; Patton, R. L.; Kirchner, R. M. *Nature* **1978**, *271*, 512. (b) Kokotailo, T.; Lawton, S. L.; Olson, D. H.; Meier, W. M. *Nature (London)* **1978**, *272*, 437−438. (c) Olson, D. H.; Kokotailo, G. T.; Lawton, S. L.; Meier, W. M. *J. Phys. Chem.* **1981**, *85*, 2238−2243.

10.1021/ja001712s CCC: $19.00
Published on Web 11/10/2000

Chart 1. Schematic Representation of the External Surface (top, left) and the Internal Surface (top, right) of a MFI Zeolite and Minimum Molecular Cross Sections for pMeDBK (bottom, left) and oMeDBK (bottom, right)

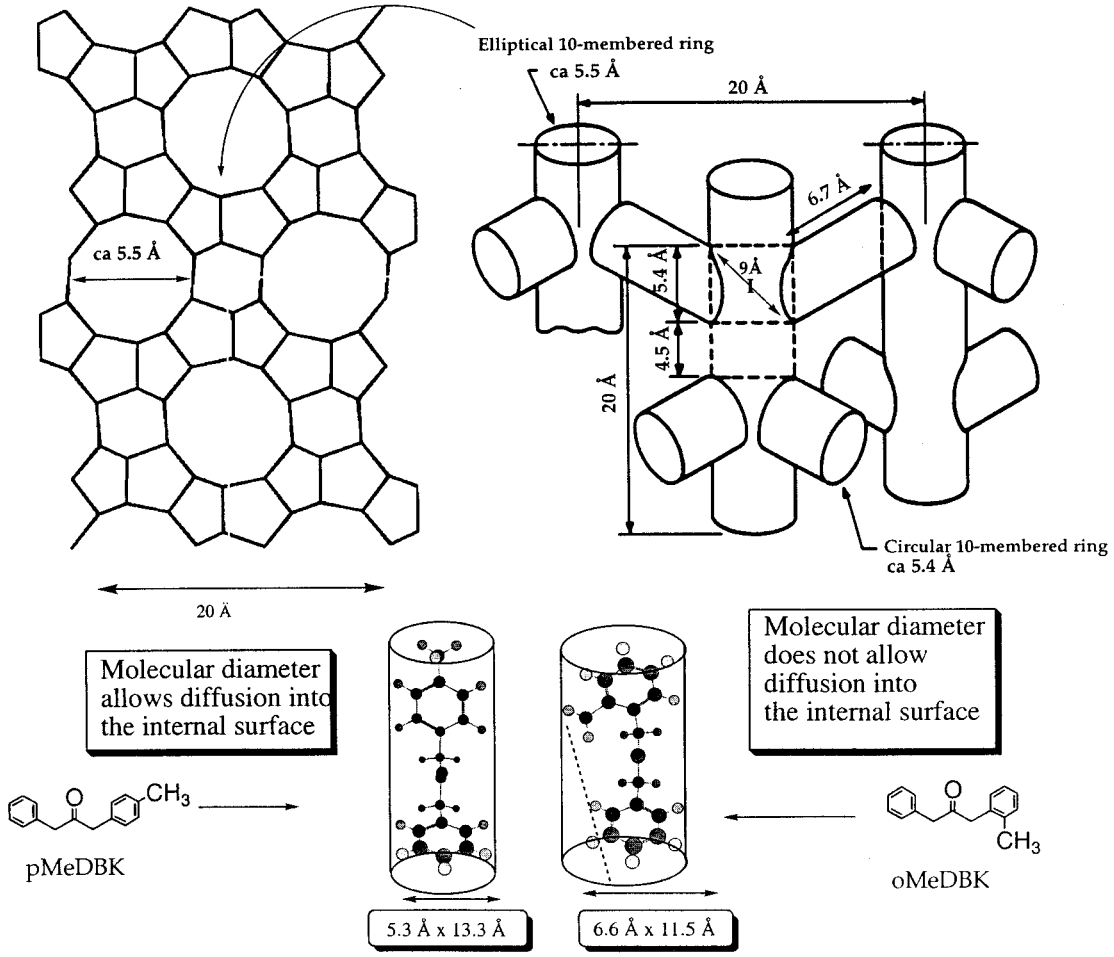

in our study the Si/Al ratios are both 20. Throughout this report, the Na (nonacidic) forms of ZSM-5 and LZ-105 are employed.

Silicalite Surface Structure: General Considerations. The salient features of the surface of silicalite (and all MFI zeolites) to be noted in Chart 1 are (1) the void space of silicalite is three-dimensional and the void space topology consists of straight (linear) channels running parallel to the [010] face and sinusoidal channels running parallel to the [100] face and (2) the pores on the [010] face have a roughly spherical shape whose diameter is ca. 5.5 Å, whereas the pores on the [100] face have a roughly elliptical shape with dimensions of ca. 5.1 × 5.4 Å^2. Throughout this report we shall use the [010] face as an example of the external surface of a MFI zeolite.

In this report we investigate the photochemistry of dibenzyl ketones (DBKs) adsorbed on zeolites.[6] The benzene ring is a critical building block of the guest DBKs examined and of the reactive radical intermediates that are generated by photochemical excitation of the guests. Thus, we are interested in characterizing the portions of the external and internal surface which are kinetically accessible *at room temperature* to guest molecules whose minimum molecular cross sections are of the order of simple alkyl benzenes.[7]

Structural Characteristics of the External Surface of MFI Zeolites. The *external surface* of a MFI zeolite crystal (Chart 1) possesses two plausible sites for binding of DBK guest molecules: (1) the "soft" and penetrable holes on the external surface, which are expected to be size and shape selective for binding of guest molecules, and (2) the "hard" impenetrable external surface framework of the zeolite crystal, which is not expected to be size or shape selective for the binding of guest molecules.

Structural Characteristics of the Internal Surface of MFI Zeolites. The *internal* void space (Chart 1) of MFI zeolites may be characterized by distinct "cavities" that can serve as adsorption sites for molecules whose molecular cross sections are of the order of *p*-xylene. The largest void space is provided by the intersections of the straight and zigzag channels which are roughly spherical with a diameter of ca. 9 Å. For a molecule with the dimensions of DBK, the entire internal surface is saturated at ca. 14 wt %/wt, ketone@zeolite.[8] The limiting saturation point for adsorption of a ketone is expected to decrease as the number and size of the cations increase (in the case of ZSM-5 or LZ-105).

Supramolecular Structure and Dynamics of Ketone@Zeolite Complexes. The working model assumed for external surface coverage is the following. Guest molecules may bind at one of two sites (Chart 1), i.e., the pores or "holes" on the external surface or the framework surface between the pores. Molecules that bind in the holes are compelled to assume a stereochemistry for which the long cylindrical axis of the ketone is perpendicular to the (idealized) plane of the external surface.

(6) (a) Turro, N. J.; Lei, X.; Cheng, C. C.; Corbin, D. R.; Abrams, L. *J. Am. Chem. Soc.* **l985**, *107*, 5824. (b) Turro, N. J.; Cheng, C. C.; Abrams, L.; Corbin, D. R. *J. Am. Chem. Soc.* **l987**, *109*, 2449. (c) Turro, N. J. *Pure Appl. Chem.* **1986**, *58*, 1219.

(7) Dessau, R. M. *ACS Symp. Ser.* **1980**, *135*, 123.

(8) Turro, N. J.; Wan, P. *J. Am. Chem. Soc.* **1985**, *107*, 678.

The size/shape characteristics of pMeDBK (Chart 1) allow this molecule relatively easy kinetic access to the internal surface through the pores on the external surface. In addition, pMeDBK is expected to have kinetic access to the intersections and channels of the internal surface at ambient temperature. The working model for the supramolecular structure of the internal surface assumes that ketone molecules favor diffusion through the linear channels and that siting in intersections is favored because they provide the largest void space.

In contrast, oMeDBK (Chart 1) possesses a molecular cross section that is slightly conical with one end of the cone having a dimension of ca. 6.6 Å in diameter and the other end having a dimension of ca. 5.3 Å in diameter. The smaller (benzyl) moiety of the cone can penetrate and intercalate in the pores of the external surface, but the (oMebenzyl) moiety is too large to penetrate the internal surface at a significant rate at room temperature. Thus, the oMeDBK molecules are capable of "plugging" the pores on the external surface if the benzyl moiety is adsorbed in the holes on the external surface. Following this logic and the paradigm for the photochemistry of DBKs (vide infra), photolysis of an oMeDBK adsorbed in the holes of the external surface is expected to produce a benzyl radical that is adsorbed in the holes and, therefore, disposed to be readily adsorbed into the internal surface and a oMebenzyl radical that can diffuse on the external surface but cannot penetrate the internal surface.

The internal surface area[9] of a crystal of a MFI zeolite is generally of the order of 500 m^2/g, and is only weakly dependent on the crystal size of the zeolite for crystals whose size is 1 μm or larger. The external surface of a crystal of a MFI zeolite, however, depends strongly on the crystal size. The external surface area of a MFI zeolite may be determined experimentally through mercury porosimetry,[10] or by the computation of the surface coverage, which requires an assumed model and comparison to experimental data.

A silicalite sample with an external surface area of 10 m^2/g will possess an external surface consisting of ca. 20% "holes" and ca. 80% external framework "surface". From these data we estimate that the holes on such a surface will be filled at a loading of ca. 0.003 g or ca. 0.3 wt %/wt (ca. 1×10^{19} molecules) when oMeDBK is adsorbed on a sample of a MFI zeolite whose surface area is 10 m^2/g. A monolayer will form at higher loadings when oMeDBK molecules are bound on the holes and the framework of the external surface. Assuming that the oMeDBK molecules bind flat on the surface, it is estimated that a monolayer will occur at ca. 0.6 wt %/wt loading for a sample of a MFI zeolite whose surface area is 10 m^2/g.

Paradigm for the Photolysis of oMeDBK@MFI and pMeDBK@MFI. A working paradigm for the photolysis of oMeDBK@MFI and pMeDBK@MFI has been shown[6] to be available from the interpretation of the observed product distributions as resulting from a mix of three processes (eqs 1−3, where, for convenience, we use the notation pACOB for

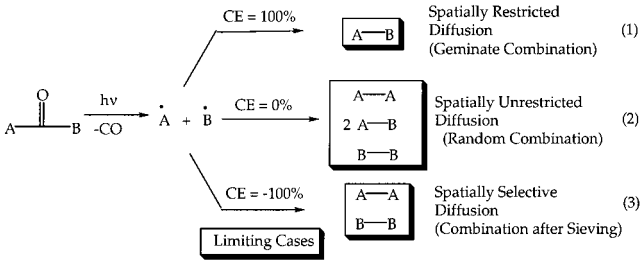

pMeDBK, and oACOB for oMeDBK): geminate combination, combination after sieving, and random combination. Consideration of the experimental product distribution as a mix of these three processes allows the product mixtures to be expressed in terms of the "cage effect" (CE) which characterizes the extent to which each of the three limiting situations of eqs 1−3 contribute to a particular experimental situation. The mechanistic interpretation, in turn, provides information concerning the supramolecular structure and diffusional dynamics of the radicals produced by photolysis of ketone@MFI.

For example, the observation of only AB as product (eq 1, CE = +100%) implies that the radicals produced by ketone photolysis are initially sited in a supramolecular structure that restricts irreversible diffusional separation of the geminate radical pair, A/B. The formation of an equal mixture of AA and BB together with the absence of AB (eq 2, CE = −100%) implies that the radicals produced by ketone photolysis are sited in a supramolecular structure which allows for the efficient diffusional separation of the geminate radical pair, A/B, and also favors the selective diffusional dynamics of sieving of A from B. The formation of a statistical 1:2:1 mixture of AA, AB, and BB (eq 3, CE = 0%) implies that the radicals produced by ketone photolysis are sited in a supramolecular structure that allows the efficient irreversible diffusional separation of the geminate radical pair, A/B, and which favors unrestricted diffusion dynamics of the radicals so that radical recombination occurs in a random and nonselective manner. From these definitions, the experimental range of CE is +100% to −100% and may be computed directly from the experimental ratio of the products of photolysis. For any specific experiment, the observed values of CE may be interpreted in terms of some specific combination of the limiting pathways of eqs 1−3 and the values of CE may be related to the supramolecular structure of the ACOB@MFI complex and the diffusional dynamics of the radicals produced by photolysis.

Results and Discussion

Photochemistry of oMeDBK and pMeDBK Adsorbed on MFI Zeolites. The observed photochemistry of oMeDBK@MFI and of pMeDBK@MFI zeolites is summarized in eqs 4−6. For pMeDBK@MFI the major product (eq 4) under all coverages investigated is pAB (positive CEs of 80% or greater) for all three zeolites. However, for oMeDBK@MFI the major products are a function of coverage (Figure 1) for the three zeolites

(9) Davis, M. E.; Lobo, R. F. *Chem. Mater.* **1992**, *4*, 756−768. Breck, D. W. *Zeolite Molecular Sieves: Structure, Chemistry, and Use*; Wiley and Sons: London, 1974. Meier, W. M.; Olson, D. H. *Atlas of Zeolite Structure Types*; Butterworth-Heinemann: London, 1992. Szostak, R. *Molecular Sieves: Principle of Synthesis and Identification*; Van Nostrand Reinhold: New York, 1989.

(10) (a) The surface area (SA) of the samples was determined by mercury porosimetry. For a description of the method see: Abrams, L.; Keane, M.; Sonnichsen, G. C. *J. Catalysis* **1989**, *115*, 410. (b) The external area available to a oMeDBK molecule on the [010] MFI external surface (2 unit cells in the *a* and *b* directions and 1 unit cell in the *c* direction) was determined by computer simulation. The variation in surface area of the ketone differs by a factor of ca. 3 depending on the specific orientation of the ketone relative to the surface and leads to an evaluation of the computation. Assuming an area of 100 $Å^2$ for a DBK molecule, and taking the average of the limiting orientations of the oMeDBK molecules on the external surface, a monolayer of oMeDBK corresponds to ca. 0.4 wt % for silicalite and ca. 1.2 wt % for ZSM-5. Modeling the external surface of a unit cell as a flat face-centered lattice with two 7 Å holes on it, the two-dimensional external surface consists of approximately equal portions of "holes" and flat surface between the holes. (c) The chemical structure of the flat surface is assumed to be composed of (relatively weakly binding) silane groups and (relatively strongly binding) silanol groups. The holes leading to the internal surface may also bind the smaller benzyl group of oMeDBK.

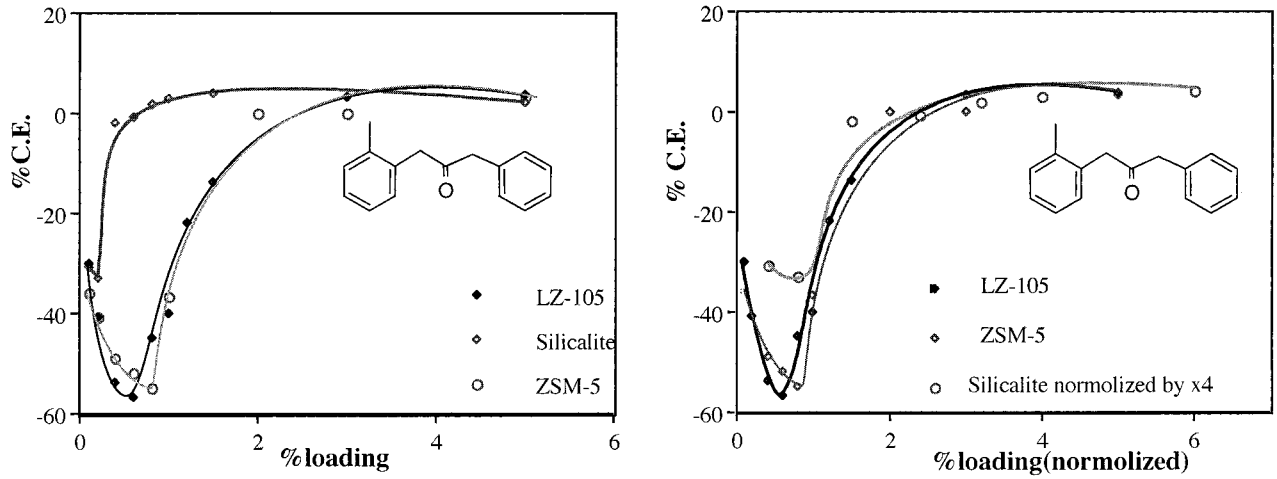

Figure 1. Cage effect (CE) vs percent of wt/wt (ketone/zeolite) loading of oMeDBK for silicalite, ZSM-5, and LZ-105 (left). The cage effect in the photolysis of oMeDBK vs silicalite loading normalized by a factor of 4 to take into account the smaller surface area of the silicalite sample (right). The error limits are estimated to be 5%.

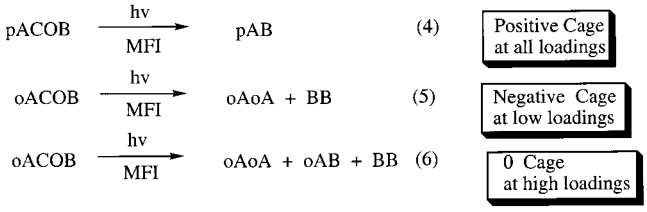

investigated. At low coverage (eq 5) the major products are oAoA and BB (negative CE), but and at higher coverages (eq 6) oAB becomes an increasingly important component of the product mixture, and at even higher coverages the products tends toward a 1:2:1 mixture of oAoA:oAB:BB (CE of 0%).

The CE for the photolysis of oMeDBK and pMeDBK was measured for compositions ranging from ca. 0.1 wt %/wt ketone@zeolite to ca. 5 wt %/wt ketone@zeolite for samples of the MFI zeolites, silicalite, ZSM-5, and LZ-105. From the working structural model discussed above, these compositions may correspond to coverages from less than a monolayer to multilayers for the external surface, and from less than a monolayer to close to ca. 30% coverage of the internal surface of the samples.

The observation of a strong positive CE for pMeDBK@MFI found for all three zeolites and for the range of coverages examined is consistent with the adsorption of pMeDBK on the internal surface in the intersections and channels (Chart 2 B). The geminate pairs produced by photolysis in the channels and intersections of the internal surface will behave in a certain degree of diffusional motion, but will be constrained from separating irreversibly and becoming free radicals. Thus, a strong positive CE is expected at all coverages of the internal surface, until saturation (ca. 14%) is achieved. However, since the cage effect is not 100%, it can be concluded that a certain small fraction of the geminate pairs become free radicals which eventually undergo random combination.

In contrast, for oMeDBK@MFI, the CE varies significantly as a function of coverage in the range 0.1% to 5 wt %/wt (Figure 1). For each zeolite (silicalite, ZSM-5, and LZ-105) at low coverages, the CE is negative. As coverage increases, the CE first drops to slightly lower values and then becomes less negative, reaching a plateau value of 0% at the highest coverages. The CE/loading profiles are identical within the experimental error for the ZSM-5 and LZ-105 samples (Figure 1), but the silicalite profile is clearly different, although similar

Chart 2. Schematic Representation of the Mechanism of Photochemistry of Adsorbed Ketones (see text for discussion) on MFI Zeolites: (A) oMeDBK at Low Coverage (left) and at High Coverage (right); (B) pMeDBK at All Coverages below Saturation of the Internal Surface

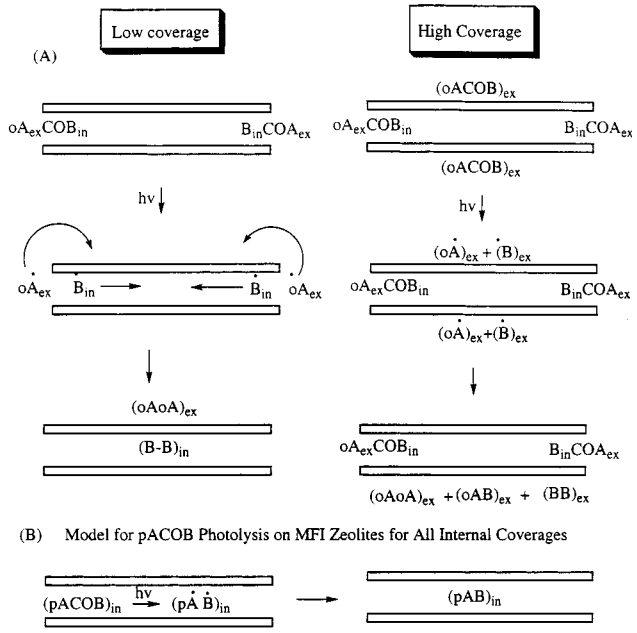

in sensitivity to loading. The ZSM-5 and LZ-105 samples show a "minimum" in the CE.

Consider the results for photolysis at low coverages for which the CE is negative.[12] The results are consistent with the following model shown in Chart 2. At low coverages (Chart 2A, left), the benzene (B) ring of oACOB intercalates into a hole on the external surface to produce a supramolecular structure $oA_{ex}COB_{in}$@MFI. Photolysis of $oA_{ex}COB_{in}$@MFI produces, after rapid decarbonylation, a secondary radical pair consisting of a B_{in} bound to a hole and a oA_{ex} radical that is free to diffuse on the external surface. The products are determined by the diffusional pathways available to the *two spatially distinct radicals*, oA_{ex} and B_{in}. The B_{in} in the hole is well positioned to diffuse into the internal surface where it will only encounter B_{in} radicals from other photolyses, but will not

(11) Turro, N. J. *Acc. Chem. Res.* **2000**, *33*, 637−646.

encounter oA_{ex} radicals, which are denied access to the internal surface. When two B_{in} radicals encounter at an intersection of the internal surface, there is sufficient space for $B_{in} + B_{in}$ radical−radical combination to produce $(BB)_{in}$. However, the oA_{ex} radicals diffuse on the external surface where they encounter other oA_{ex} radicals to produce $(oAoA)_{ex}$. Thus, when only the holes are occupied (Chart 2B, left), $(oAoA)_{ex} + (BB)_{in}$ are the major products of photolysis and the result is a strong negative cage effect.

We now explain the reason for the increase in the CE as the loading increases from strong negative values to a limiting value of 0. It was shown above that ca. 20% of the accessible external surface is available for binding of oMeDBK molecules in holes. After the holes are filled additional ketones must adsorb on the framework until a monolayer and then multilayers are produced. The observation (Figure 1) that as the loading increases, the CE approaches zero, implies that sieving is becoming less efficient and random radical combination is becoming dominant on the external surface at the higher loadings. This result is to be expected from Chart 2 if the increased loading first causes the holes on the external surface to be "plugged" by the oA_{ex}-COB_{in} molecules. As the loading of the fraction of $oA_{ex}COB_{ex}$ molecules increases, the fraction of ketones in holes decreases and an increasingly greater fraction of photolyzed ketones produce oA_{ex} and Be_x radicals which are able to randomly diffuse and combine randomly on the external surface. These B radicals produced by ketones photolyzed on the framework are inhibited from sieving into the internal surface because the holes are plugged by the oMeDBK ketones adsorbed in the holes and the result is a zero cage effect in the limit.

Surface Area Analysis of Photochemical Data. Although the results in Figure 1 are quantitatively similar for all three zeolites, the results for the silicalite are "offset" from those for the ZSM-5 and LZ-105 samples, which are experimentally indistinguishable. In particular, the sensitivity of the CE to loading for silicalite is similar to that for the other two zeolites, but is "displaced" to lower loadings. These results are readily interpreted in terms of external surface area (SA) differences of the zeolites. Indeed, from surface area measurements by mercury porosimetry, the SA of the silicalite sample (5 m^2/g) is less than the LZ-105 (10 m^2/g) and ZSM-5 (15 m^2/g) samples.

For low loadings, conditions for which the available SA and number of holes determine the CE, a linear fit of the data yields values of ca. 0.5% and 2% for the loadings at which a CE of 0% is achieved (assumed to correspond to the formation of a monolayer, Figure 1) for the silicalite and ZSM-5 samples, respectively. This ratio of 4 at which the CE becomes 0 is of the same order, 2−3, of the experimentally measured[10] SAs of the silicalite compared to the LZ-105 and ZSM-5 samples. Furthermore, computational determination of the relationship between the loading and the surface coverage of oMeDBK shows that (depending on the orientation of the ketone with respect to the surface) a monolayer of ketone is expected to occur for loading of 0.2−0.6 wt/wt % for the silicalite sample and 0.7−1.8% for the ZSM-5 sample. These computational values are in qualitative correspondence with those obtained from experimental analysis of the loading dependence of the cage effect and the supramolecular model (Chart 2) employed to analyze the data.

Thus, based on the photochemical results, we conclude that not only is the model of Chart 2 consistent with the data, but that the variation of the CE as a function of loadings for different zeolites is a direct result of the number of holes available for binding of oMeDBK on the external surface. Thus, the data can be interpreted within the framework of an equilibrium adsorption on an interface. We now consider and analyze the spectroscopic and adsorption isotherm data within the framework of this paradigm, based on the photochemical product yields, to determine if an equilibrium adsorption is an appropriate model to explain the photochemical data.

^{2}H NMR Results. ^{2}H NMR is an excellent probe of molecular motion in the solid state, since the form of the observed ^{2}H NMR spectra can be simulated based on assumed motional models and compared to experimental data.[13] The molecular motion of an adsorbed DBK molecule will depend on how it is bound to the zeolite (holes, external framework, internal channels, or intersections). Furthermore, if the binding characteristics of a ketone@MFI system change as a function of loading, this supramolecular structural change may be monitored by ^{2}H NMR, and these inferred structural changes can be compared to those employed to interpret the photochemical results.

The ^{2}H NMR spectra of oMeDBK-d_5 and pMeDBK-d_5 adsorbed on MFI samples were obtained for compositions from ca. 0.5 wt %/wt (lower limit determined by signal-to-noise considerations) to ca. 10 wt %/wt DBK@MFI (upper limit determined by maximum coverage of the internal surface). Some examples of the resulting spectra are shown in Figure 2 for a low (1wt %/wt), intermediate (5wt %/wt) and high (10wt %/wt) loading for each ketone adsorbed on ZSM-5. Similar ^{2}H NMR spectra were observed for adsorption of each ketone on silicalite and LZ-105.

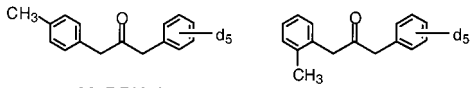

pMeDBK-d_5 oMeDBK-d_5

The spectra in Figure 2 may be interpreted qualitatively[13] based on the relationship between the width at half-heights ($\Delta H_{1/2}$) of spectra and the limits of molecular motion for ^{2}H NMR: (1) in the fast motion limit, $\Delta H_{1/2}$ values of the order of <1 kHz are expected, and (2) in the slow motion limit, $\Delta H_{1/2}$ values of the order of ca. 140 kHz are expected. Since the

(12) We note that at the lowest coverages for the ZSM-5 and LZ-105 samples, although the cage effect is negative at all measurable coverages, it begins to become less negative (more positive) at the lowest loadings for which data could be obtained. The origin of this "positive" cage effect is not clear, but could be due to scavenging by adventitious trace amounts of oxygen in the sample (which will become more pronounced as the amount of sample decreases), or to a certain fraction of adsorption on defect sites that favor a positive cage effect. However, an interesting mechanistic possibility is that at low loadings where there are many pore openings that are not occupied by an adsorbed ketone molecule, some of the B radicals that have diffused to the internal surface may escape to the external surface where they combine with oA radicals. This leads to an increase in the amount of oAB formed in the product mixture and the computed CE is more positive. As the loading of the AB ketone is increased, there are fewer openings to the surface and the B radicals will combine increasingly more exclusively on the internal surface. This process continues as the ketone loading increases until all of the pores' openings to the surface are plugged with ketones. At this loading (CL), the minimum CE is observed. From this point photolysis involves both ketones in the pores and ketones on the external framework. Increasing addition of ketone increases the fraction of ketones photolyzed on the external framework. These ketones produce a CE of zero.

(13) (a) For a discussion of the relationship between motion and line shape, see: Wittebort, R. J.; Olejniczak, E. T.; Griffin, R. G. *J. Chem. Phys.* **1987**, *86*, 5411. Mantxsh, H. H.; Sato, H.; Smith, I. C. P. *Prog. NMR Spectrosc.* **1977**, *11*, 211. Hoatson, G. L.; Vold, R. L. *NMR Basic Principles and Progress*; Springer; Berlin, 1994; p 32. (b) Examples of the use of ^{2}H NMR to investigate the adsorption of *p*-xylene on ZSM-5 and leading references: Eckman, R. R.; Vega, A. J. *J. Phys. Chem.* **1986**, *90*, 4697. Kustanovich, I.; Vieth, H. M.; Luz, Z.; Vega, S. *J. Phys. Chem.* **1989**, *93*, 7427.

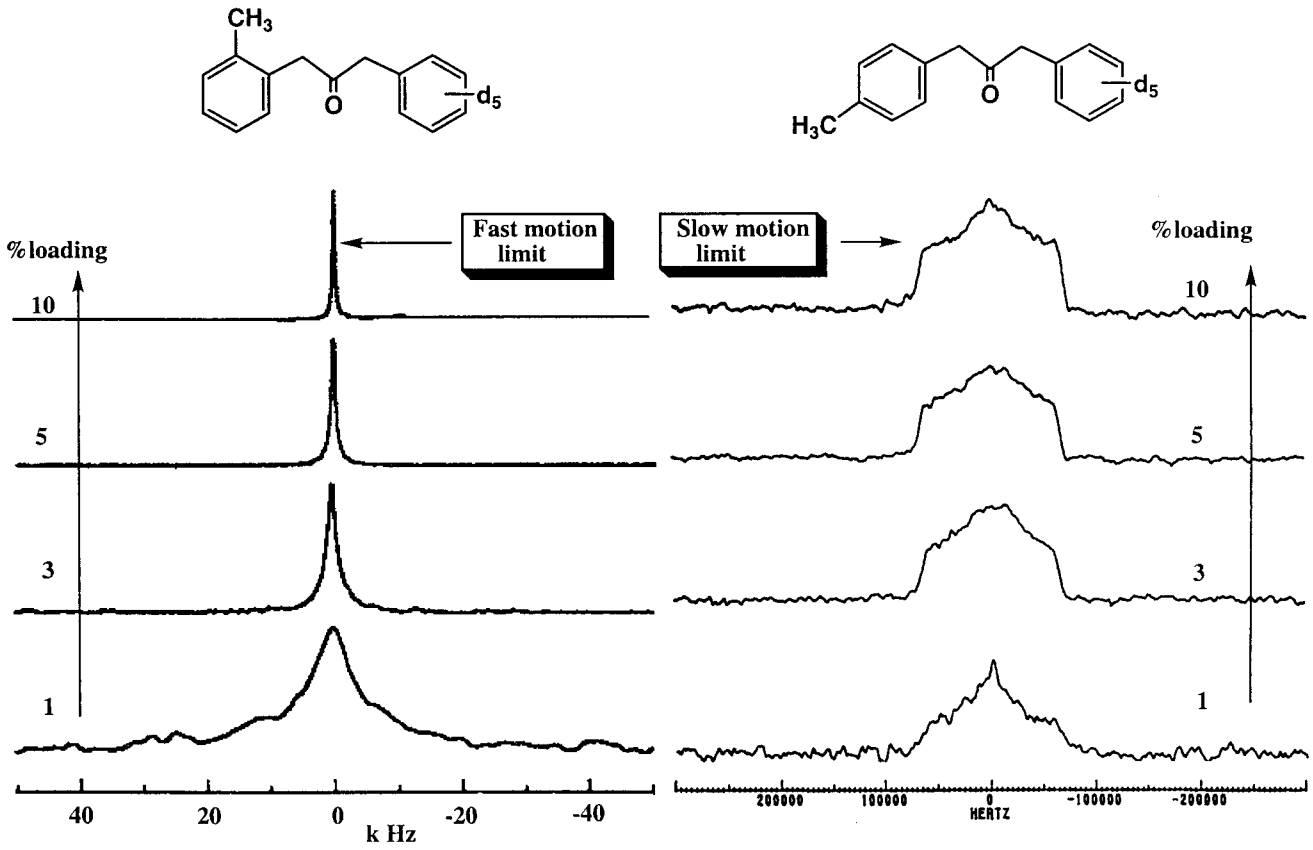

Figure 2. ^{2}HNMR spectra of oMeDBK-d_5 (left) and pMeDBK-d_5 (right) adsorbed on ZSM-5. Indicated loadings are wt %/wt (ketone/zeolite). The heights of the spectra are normalized for clarity.

motion of adsorbed molecules will depend on the supramolecular structure, the $\Delta H_{1/2}$ values carry information on the sites to which the ketones (and products bearing ^{2}H atoms) are located.

The $\Delta H_{1/2}$ values of the ^{2}H NMR spectra for pMeDBK-d_5 are very broad under all compositions and are close to the theoretical limit for slow motion broadening (ca. 140 kHz). As saturation is approached, the ketone is strongly constrained and the width of the ^{2}H NMR signal is close to that of a rigid solid. The increase in broadening with increased loading (Figure 2) is attributed to the constraints on the motion of ketones as the internal surface is increasingly filled with ketones. These results are expected when pMeDBK is adsorbed and constrained to the cages and intersections of the internal surface.

In contrast to the results for pMeDBK-d_5, the $\Delta H_{1/2}$ values of the ^{2}H NMR spectra for the oMeDBK-d_5 samples vary from values of ca. 14 kHz (intermediate motion) at ca. 1% composition to less than 1 kHz (approaching the limit for fast motion) at 10% composition. The ^{2}H NMR results are consistent with the working model for the photochemistry of oMeDBK@MFI (Chart 2), which assumes the holes are filled first and then the framework of the external surface for oMeDBK@MFI. For up to ca. 0.5% loading of oMeDBK on the ZSM-5 zeolite (and LZ-105), the ^{2}H NMR spectrum shows a $\Delta H_{1/2}$ value of ca. 14 kHz, which is ascribed to oMeDBK-d_5 molecules adsorbed with the phenyl-d_5 ring plugged in the holes of the external surface; a constant value of $\Delta H_{1/2}$ is observed as the holes are being filled. After the holes are filled, the next ketones added adsorb on the external surface until a monolayer and then multilayers are formed. The latter create a relatively liquid interface in which oMeDBK-d_5 molecules are adsorbed. The ^{2}H NMR spectrum sharpens and approaches the fast motion limit of less than 1 kHz as oMeDBK molecules are adsorbed first in the monolayer and then in a multilayer.

For pMeDBK the ^{2}H NMR signals for all three zeolites studied are all very similar and in the slow motion domain. However, for oMeDBK there are quantitative differences between silicalite and the ZSM-5 (and LZ-105) samples due to differences in the external surface area. These differences will be discussed further after an analysis of the results of an EPR probe of the supramolecular structure of the ketone@MFI systems is made.

EPR Probe Investigation of Adsorption. ^{2}H NMR provides a *direct* spectroscopic analysis of the supramolecular binding of oMeDBK-d_5 and pMeDBK-d_5 to the external surface and internal surface, respectively, of MFI zeolites. We now compare the ^{2}H NMR results with those of an *indirect* EPR nitroxide probe.[14] The strategy of this indirect method is to start with an EPR probe whose structure only allows binding to the external surface and to observe the EPR spectrum of the probe as a function of added ketone. If the ketone is adsorbed on the external surface, it will influence the EPR spectrum of the probe. If the ketone is adsorbed on the internal surface, it will *not* influence the EPR of the probe.

4-Oxo-Tempo (T) was selected as the indirect EPR probe of the adsorption of pMeDBK and oMeDBK to MFI zeolites. The molecular cross section of T prevents its absorption into the internal surface, but a portion of this molecule can fit into the holes of the external surface (as is the case for oMeDBK) and can be adsorbed on the external framework. According to the working model, pMeDBK, which is bound to the internal surface, should not influence the EPR spectrum of T, which is

(14) Berliner, L. J., Ed. *Spin Labeling. Theory and Applications*; Academic Press: New York, 1973.

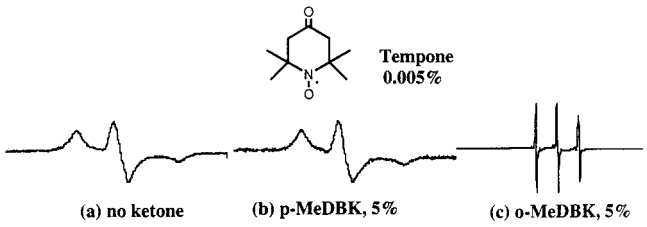

Figure 3. EPR spectra of tempone (T) at 0.005 wt %/wt loading on silicalite: (left) T alone; (middle) T plus 5% coadsorbed pMeDBK; and (right) T plus coadsorbed oMeDBK.

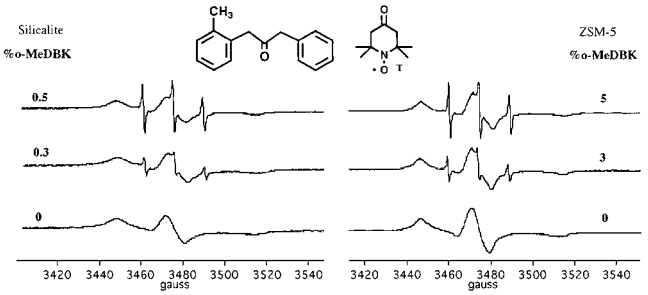

Figure 4. EPR spectra of oMeDBK coadsorbed with 0.005% T on silicalite (left) and ZSM-5 (right) as a function of loading of ketone.

adsorbed on the external surface. On the other hand, oMeDBK, which is bound to the external surface, may influence the EPR spectrum of T, i.e., if it can displace T from its initial binding site to a second one which exhibits a different EPR signal.

Figure 3 shows the EPR spectra in the absence (Figure 3, left) of coadsorbed ketone, in the presence of coadsorbed pMeDBK (5%, Figure 3, middle), and with coadsorbed oMeDBK (5%, Figure 3, right). The EPR spectrum of T in the absence

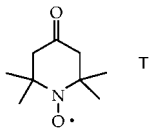

of ketone displays the broad features of a probe that is in slow motion, indicating a strong binding to the zeolite external surface. The coadsorption of pMeDBK does not influence the probe EPR spectrum. However, the coadsorption of oMeDBK has a dramatic influence on the probe EPR spectrum, transforming it from one characteristic of a nitroxide in slow motion to the characteristic sharp three-line spectrum of a nitroxide in fast motion (Figure 3c).

Given the high sensitivity of the probe samples to coadsorbed oMeDBK, the EPR spectra for fixed low composition of T (0.005%) were measured as a function of loading of oMeDBK. Figure 4 shows representative spectra of T adsorbed on silicalite (Figure 4, left) and ZSM-5 (Figure 4, right) in the presence and absence of coadsorbed oMeDBK. The EPR spectra of T were very sensitive to the loading of oMeDBK. The observed spectra can be described as the superposition of two components, "fast" (sharp features) and "slow" (broad features), due to slow exchange of the probes in two environments.

The compositional dependence of the two components in the EPR spectra of T adsorbed on ZSM-5 and LZ-105 is almost quantitatively identical. However, for the silicalite sample, the results show that the onset of the fast component occurs at ca. 0.16% loading for the silicalite sample and at ca. 1.2% for the ZSM-5 (and LZ-105) sample. This result is reminiscent of the differences in the silicalite and ZSM-5 (and LZ-105) samples for the photochemical results (Figure 1).

Under the working hypothesis that the appearance of the "fast" component upon addition of oMeDBK is related to the same supramolecular structural features as those responsible for the photochemical results, a quantitative analysis of the coadsorbed oMeDBK on the observed EPR spectra by simulation was performed employing the well-established procedure of Schneider and Freed.[15] The simulation of the experimental spectra allows the computation of the percentage of radicals that are in environments that constrain the probe to slow motion conditions on the EPR time scale (1 ns $< t_c <$ 500 ns) and also the percentage of radicals in the fast motion regime ($t_c <$ 1 ns). Finally, simulation of the spectra allows the computation of the fraction of the radicals that are close enough to be in the limit of fast spin−spin exchange.

The percent of T radicals in the fast motion regime is plotted (semilog because of the range) as a function of coverage on the left ordinate of Figure 5 (silicalite, left; ZSM-5, right). For comparison, the values of the inverse of the $\Delta H_{1/2}$ values of ^{2}H NMR spectra ($1/\Delta H_{1/2}$) are plotted on the right ordinate. The correspondence of the EPR and ^{2}H NMR for all loadings on the silicalite and for loadings above ca. 1−2% for the ZSM-5 is striking, i.e., the response of the two spectroscopic methods to loading is very similar and therefore the two magnetic resonance methods are probing the same supramolecular features of the binding of oMeDBK to the external surface. Indeed, it should be noted that the response of the binding of oMeDBK to loading, as measured by either of the spectroscopic methods is similar, *the onset of the fast motion is displaced by a factor of ca. 4 for the silicalite and ZSM-5 samples*. This is consistent with the surface area differences of ca. 4 of the samples, i.e., the silicalite with a smaller external surface area has fewer holes so that adsorption of oMeDBK on the framework starts at a lower loading. Thus, the differences between silicalite and ZSM-5 (and LZ-105) can be attributed entirely to the difference in the surface area of the two samples, a result completely consistent with the photochemical results.

Direct EPR Analysis of Photolyzed Samples: Persistent Benzyl Radicals. According to the conclusions above, benzyl radicals are produced from photolysis of oMeDBK in the holes and then absorbed in the internal surface. Also, the observation that the CE is slightly less than +100% from the photolysis of pMeDBK indicates that a small fraction of free radicals is produced from some of the geminate pairs produced from the photolysis of pMeDBK. It is therefore possible that benzyl radicals adsorbed on the internal surface might become persistent[16] and be observable by direct EPR analysis.

Samples of oMeDBK and pMeDBK adsorbed on silicalite, ZSM-5, and LZ-105 were photolyzed under vacuum. Several minutes after photolysis, the samples were analyzed directly by EPR spectroscopy. All the samples displayed EPR signals lasting several hours (Figure 6); thus the radicals are "persistent".[16] Upon addition of air to the samples, the spectra of the benzyl radicals were completely transformed into peroxy radicals.[17] The EPR spectrum (Figure 6 left, bottom) produced by photolysis of oMeDBK could be assigned *exclusively* to the

(15) Schneider, D. J.; Freed, J. H. In *Biological Magnetic Resonance. Spin Labeling. Theory and Applications*; Berliner, L. J., Reuben, J., Eds.; Plenum Press: New York, 1989; Vol. 8, p 1.

(16) Griller, D.; Ingold, K. U. *Acc. Chem. Res.* **1976**, *9*, 13−19. For examples of persistent radicals produced in zeolite from ketone photolysis, see: (a) Turro, N. J.; Lei, X.; Li, W.; McDermott, A.; Abrams, L.; Ottaviani, M. F.; Beard, H. S. *Chem. Commun.* **1998**, 695−696. (b) Turro, N. J.; McDermott, A.; Lei, X.; Li, W.; Abrams, L.; Ottaviani, M. F.; Beard, H. S.; Houk, K. N; Beno, B. R.; Lee, P. S. *Chem. Commun.* **1998**, 697−698.

(17) Hirano, T.; Li, W.; Abrams, L.; Krusic, P.; Ottaviani, M. F.; Turro, N. J. *J. Org. Chem.* **2000**, *65*, 1319−1330.

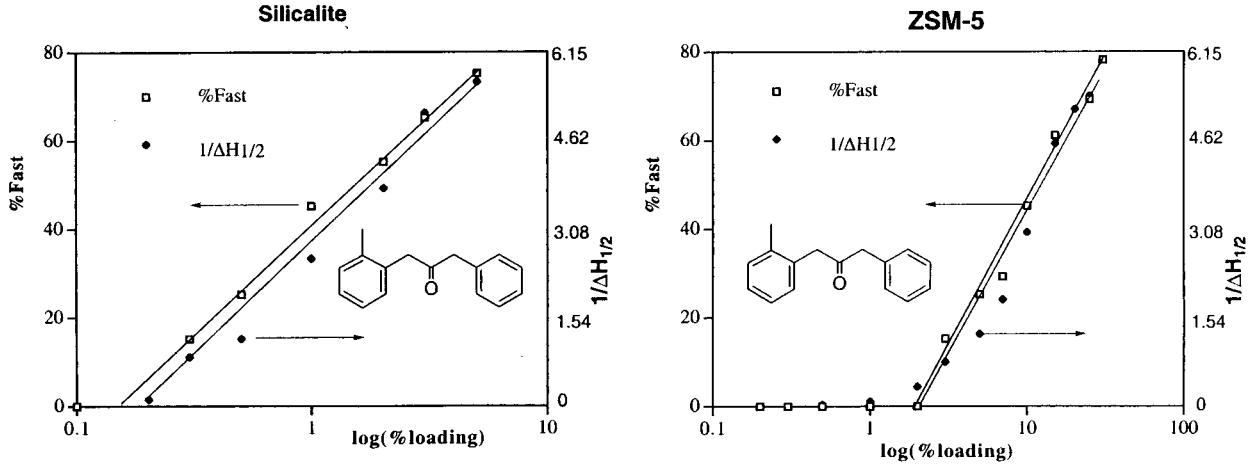

Figure 5. Semilog plot of the EPR motion parameters (left ordinate of each plot) and ^{2}H NMR motion parameter (right ordinate of each plot) as a function of loading (percent wt/wt ketone/zeolite) of oMeDBK.

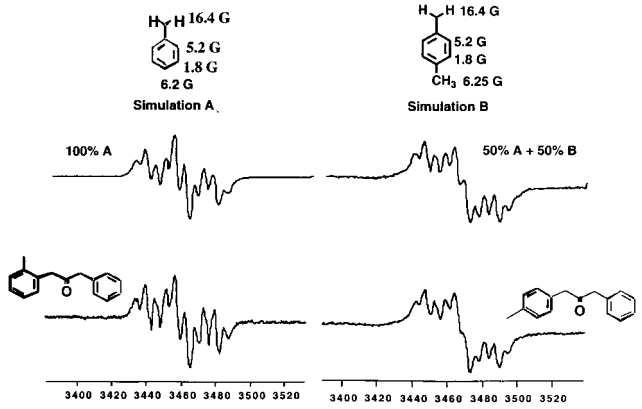

Figure 6. EPR spectra produced by photolysis of oMeDBK (lower left) and pMeDBK (lower right) adsorbed on LZ-105. The top left spectrum corresponds to the spectrum of a benzyl radical (A) fit with the indicated hyperfine coupling constants from the literature. The top right spectrum corresponds to the spectrum of a 50% mix of A and the pMebenzyl radical (B). The hyperfine coupling constants employed for the simulations are indicated.

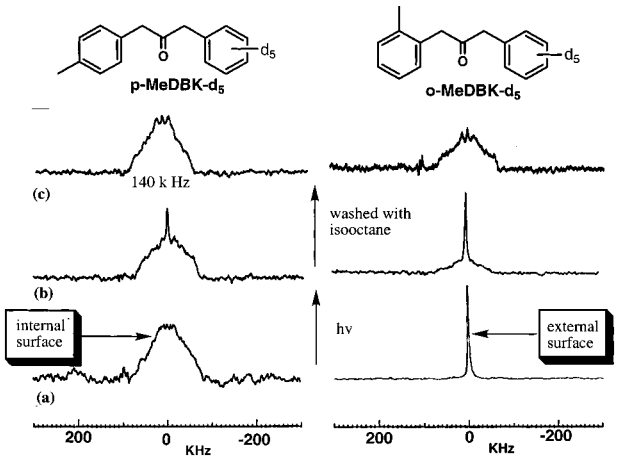

Figure 7. ^{2}H NMR spectra of in situ photolysis of oMeDBK (right) and pMeDBK (left). The ketones are adsorbed on ZSM-5 at an initial wt/wt of 3%. Spectrum a corresponds to the sample before photolysis; spectrum b corresponds to the sample after photolysis; and spectrum c corresponds to the photolyzed sample washed with isooctane.

benzyl radical based on computer simulation employing hfc constants from the literature.[18] The EPR spectrum (Figure 6 right, bottom) produced by photolysis of pMeDBK could be assigned to a mixture of benzyl radicals and pMebenzyl radicals based on computer simulation. The results for oMeDBK are consistent with the sieving of the benzyl radicals into the internal surface, which causes their persistence. The absence of oMebenzyl radicals is consistent with rapid diffusion and recombination of these radicals on the external surface.

The observation of persistent benzyl radicals from the photolysis of pMeDBK is consistent with the assumption that some of the benzyl radicals adsorbed on the internal surface escape geminate combination and become "free" and inhibited from undergoing radical−radical reactions.

In Situ Analysis of the Photochemistry of oMeDBK and pMeDBK by ^{2}H NMR. The photochemistry of oMeDBK d_5 and pMeDBK d_5 adsorbed on MFI zeolites can be investigated directly in situ by solid-state ^{2}H NMR. The results of the photolysis of oMeDBK-d_5 and pMeDBK-d_5 employing in situ ^{2}H NMR analysis are shown in Figure 7. The photolysis of oMeDBK-d_5 (Figure 7a, right) shows an initial sharp line in the ^{2}H NMR spectrum of the sample as expected for a coverage at which most of the ketones are adsorbed on the framework. Upon photolysis to partial conversion a broad line appears in addition to the original sharp line. Upon washing with isooctane (which scrubs off molecules selectively from the external surface) the sharp line is removed and only the broad line remains. Photolysis of pMeDBK-d_5 (Figure 7a, left) shows an initial broad line in the ^{2}H NMR of the sample. Upon photolysis the shape of the broad line changes slightly and a small sharp line appears. Washing with isooctane removes the sharp line.

The ^{2}H NMR results of the in situ photolysis are consistent with the working model of Chart 2. Photolysis of oMeDBK-d_5 leads to deuterated benzyl radicals which are sieved into the internal surface and eventually couple to produce 1,2-diphenylethane-d_{10}. The motion of the latter is constrained on the internal surface so that, as a product produced by photolysis, it produces a broad peak (Figure 7c, right). Thus, in the ^{2}H NMR at ca. 5% loading on ZSM-5 before photolysis, a sharp peak due to the oMeDBK-d_5 on the external surface is observed (the broad peak due to oMeDBK-d_5 in the holes is obscure and in the baseline noise). Upon photolysis the sharp peak decreases in intensity and is eventually replaced by a broad peak due to the 1,2-diphenylethane-d_{10} product that is adsorbed on the internal surface.

pMeDBK-d_5 is *initially* sited on the internal surface. Photolysis takes place on the internal surface and 1,2-diphenyl-

(18) Conradi, M. S.; Zeldes, H.; Livingston, R. *J. Phys. Chem.* **1979**, *83*, 633.

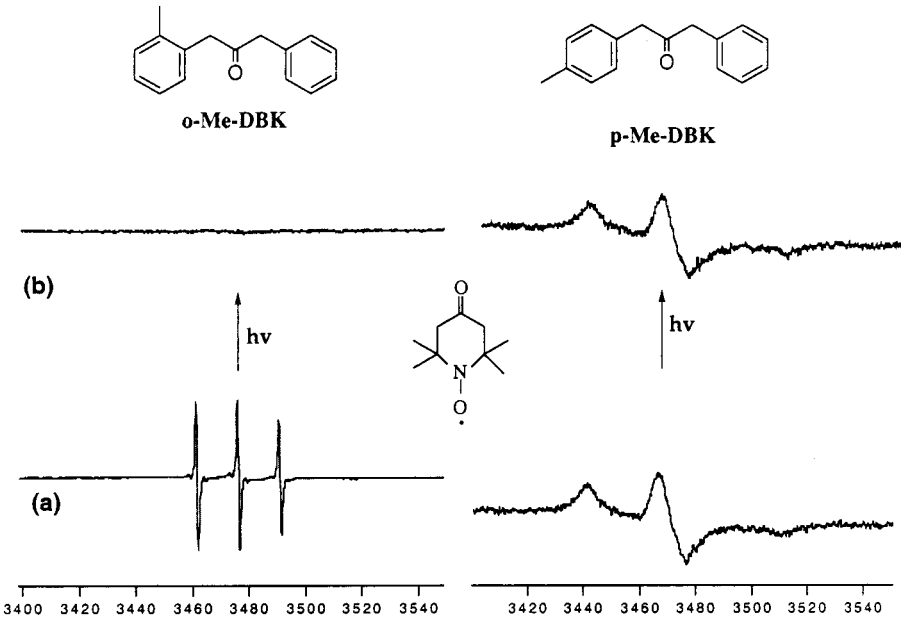

Figure 8. EPR spectra of in situ photolysis of oMeDBK (left) and pMeDBK (right) coadsorbed with T (0.01%) on silicalite at an initial wt/wt of 5%. The lower spectra correspond to the unphotolyzed sample and the upper spectra correspond to the samples after photolysis.

ethane-d_{10} is produced as the major product and is responsible for the change in shape of the broad peak (Figure 7c, left). The sharp peak in the ^{2}H NMR spectra of pMeDBK-d_5 (Figure 7 b, right) is attributed to 1,2-diphenylethane-d_{10} *that was formed on the internal surface and then diffused to the external surface*. Consistent with this interpretation is the observation that the species responsible for the peak could be completely removed (Figure 7c, left) by repeated washings with isooctane (which cannot enter the internal surface). Isooctane is also capable of washing away oMeDBK-d_5 adsorbed on the external surface leaving behind only the product 1,2-diphenylethane-d_{10} adsorbed on the internal surface.

In Situ Analysis of the Photochemistry of oMeDBK and pMeDBK by EPR. The photoreaction of oMeDBK and pMeDBK can also be investigated *indirectly* in situ by solid-state EPR of the nitroxide probe, T. The results of the photolysis of oMeDBK and pMeDBK coadsorbed with T are shown in Figure 8.

The working model suggests that the nitroxide probe, T, will be an excellent scavenger of radicals produced on the external surface, but will not be able to react with radicals produced on the internal surface. For samples of T that were coadsorbed with pMeDBK, extended photolysis produces essentially no change (Figure 8, right) in the observed broad signal of T (even though the ketone was shown to be photolyzed to product). However, when a sample containing oMeDBK coadsorbed with T is photolyzed, the sharp three-line T signal disappears rapidly (Figure 8, left). Thus, no significant fraction of benzyl radicals produced by photolysis of pMeDBK adsorbed on the internal surface exits and reacts with T, whereas T is an excellent radical scavenger for the radicals produced on the external surface by photolysis of oMeDBK.

Adsorption Isotherm for oMeDBK@MFI. All of the results reported above are qualitatively consistent with the assumption that the adsorption of oMeDBK on the external surface follows equilibrium saturation behavior, which is described by a Langmuir expression such as

$$A = MkC/(1 + kC) \qquad (7)$$

where A is the value of a parameter proportional to coverage,

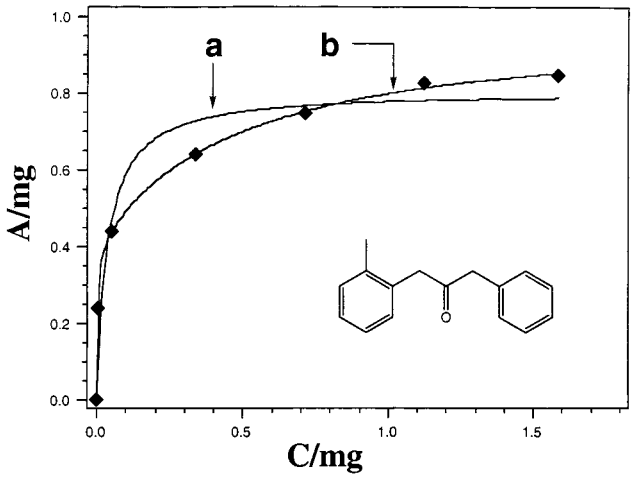

Figure 9. Langmuir isotherm analysis of oMeDBK adsorbed on LZ-105 from an isooctane solution. A (y axis) is the amount (mg) of oMeDBK adsorbed on 100 mg of LZ-105 at equilibrium, and C (x axis) is the amount (mg) of oMeDBK left in a 3 mL solution. Curves a and b were calculated by using the Langmuir isotherm eqs 7 and 8 in the text, respectively.

C is the loading of oACOB (wt/wt), M is the maximum value of A (computed from fitting the data to eq 7), and k is related to the equilibrium constant for adsorption of the ketone on the external surface. The adsorption isotherm of oMeDBK adsorbed onto LZ-105 from isooctane was measured at ambient temperature. The results are shown in Figure 9. From the results it can be seen that (curve a in Figure 9) the data do not fit the one-site model of eq 7.

Since the results of the photochemistry and magnetic resonance experiments are consistent with a two-site model of adsorption of oMeDBK on the external surface, the data were fit to the two-site model of eq 8, where the parameters have the same meaning as in eq 7 for two binding sites: site I and site II, respectively. In this case, the fit is acceptable (Figure 9, fit b). The values of M_I, M_{II}, k_I, and k_{II} were obtained from the fitting of curve b as summarized in Table 1.

$$A = M_I k_I C/(1 + k_I C) + M_{II} k_{II} C/(1 + k_{II} C) \qquad (8)$$

Table 1. Langmuir Parameters

	site I		site II	
ketone	M_I/mg	k_I	M_{II}/mg	k_{II}
oMeDBK	0.40 ± 0.02	350 ± 50	0.59 ± 0.02	2.1 ± 0.3

According to the model of Chart 2, data from the adsorption isotherm provide quantitative information on the binding strengths and fractions of oMeDBK molecules bound in the two sites, i.e., the supramolecular structure of the external surface of oMeDBK@LZ-105. From the Langmuir analysis (Table 1), the binding constant, k_I, of site I is *a hundred times larger* than k_{II} of site II, *indicating that site I has a much stronger adsorption affinity for oMeDBK than does site II on the LZ-105 external framework surface*. According to the working model, site I is the holes on the external surface and site II is the solid framework between the holes. In addition, from Langmuir analysis, the maximum amount of oMeDBK adsorbed on site I of the LZ-105 surface is ca. 0.3 mg per 100 mg of LZ-105, which corresponds to 0.3−0.5% loading, experimentally consistent with the loading expected for filling the holes from both computation and the results of photochemical and EPR analysis. Finally, the *M* values represent the fraction of surface available for binding by each site. The values of 40% and 60% can be compared to the estimated values of 20% and 80% deduced from consideration of the [010] surface. Thus, a quantitative working model of Charts 1 and 2 is supported by excellent agreement between data from several independent sources, e.g., theoretical computations, photochemical product analysis, EPR analysis, and classical isotherm analysis.

Conclusions

The results in Figures 1−9 provide convincing evidence that the same factors operate to determine the coverage dependence of the photochemical and spectroscopic parameters of oACOB and pACOB adsorbed on MFI zeolites. These factors determine the supramolecular structure and dynamics of the oACOB@MFI complex as a function of variation in supramolecular composition. In the case of oACOB, adsorption on the external surface as a function of coverage causes a continuous modification of supramolecular structure and dynamics of the ketone and the radicals produced from photolysis. At low coverage, the ketone is weakly adsorbed in the holes on the external surface. At higher coverage, as a monolayer of ketone is formed, the holes of the external surface are plugged and sieving becomes less efficient relative to diffusion in the monolayer for both the ketone and the radicals produced by photolysis.

The observation that the data for the photochemical, ^{2}H NMR, and EPR analyses for silicalite can be correlated quantitatively with those for ZSM-5 and LZ-105 by a scaling factor of ca. 2−4, which is of the order of the ratio of the measured surface areas, demonstrates that common topological factors proportional to the available external surface area operate to determine the measured parameters in each case. This correlation, in combination with measured surface areas, classical adsorption isotherms, and computed surface coverages, allows the extraction of molecular level information concerning the supramolecular structure and dynamics of molecules adsorbed on the external surface of zeolites. Such information is extremely difficult to obtain using other techniques.

In the case of pACOB, adsorption places ketones in the independent constraints of the channels and intersections of the internal surface. These constraints are strong and relatively independent of loading.

Molecular probes for which chemical activation is provided by photochemical excitation, and not by the active sites of zeolites, can distinguish surface diffusion and sieving effects based on subtle size/shape effects which control supramolecular structure and dynamics. The use of photochemistry to investigate supramolecular structure and dynamics thereby provides a simple, but powerful tool that, in conjunction with magnetic resonance spectroscopy, allows the development of a more complete molecular level description of the basis of the mechanism of size/shape separation and catalytic selectivity of molecular sieve zeolites.

Experimental Section

Materials. The synthesis of pMeDBK and oMeDBK has been reported.[20] The deuterated ketones were prepared by modification of literature procedures. Benzene-d_6 was employed to prepare[21] benzoyl-d_5 chloride, which was converted[22] to benzyl-d_5 chloride. The latter served as the precursor in the preparation[23] of pMeDBK-d_5, oMeDBK-d_5, and DBK-d_5. 4-oxo-Tempo from Aldrich was used as received. Isooctane (Aldrich) was stirred with ZSM-5 zeolite to remove the straight chain hydrocarbon impurities.

Zeolites. The silicalite (Si/Al >1000) is a product from UOP. The ZSM-5 (Si/Al = 20) is a Chemie Utikon product, obtained as a generous gift from Dr. V. Ramamurthy. The LZ-105 (Si/Al = 20) was a generous gift from Dr. Edith Flanigen of Union Carbide. The mean crystal size of the silicalite was ca. 1 μm and the mean crystal size of the ZSM-5 and LZ-105 samples was ca. 0.3 μm. The external surface area was determined by using mercury porosimetry[10]

Sample Preparation. The zeolite samples were activated in a furnace at 500 °C for 2 h. A typical preparation was as follows: A specific loading was achieved by stirring a weighed amount of ketone in a solution of 0.8 mL of isooctane with 300 mg of zeolite overnight. After evaporation of the solvent under argon flow, the samples were dried under vacuum to 2×10^{-5} Torr for the photolysis samples and 1×10^{-3} Torr for solid-state ^{2}H NMR measuring samples. GC analysis was employed to determine the photolysis products on a 25 m SE-30 column with 1-phenyldodecane as internal standard. Some photolyzed samples were washed with isooctane to remove molecules adsorbed in the zeolite's external surface.

Photolysis. Typical photolysis conditions employed 50 mg of degassed zeolite samples in a quartz cell. A 450-W medium-pressure Hanovia Hg lamp was employed as the light source for the samples for several minutes with an aqueous K_2CrO_4 (10 mm) filter (0.002 M K_2CrO_4 in 1% K_2CO_3) to isolate the 313 nm line.

Instrumentation. Solid-state ^{2}H NMR spectra were recorded on a Bruker 250 MHz spectrometer at 38.397 MHz at room temperature. EPR spectra were recorded on a Bruker ESP 300 spectrometer interfaced to a computer with Bruker ESP1600 system software. Spectrometer conditions were as follows: microwave frequency, 9.74 GHz; field modulation amplitudes, 1 G at 100 kHz; microwave power, 3.14 mW.

Mercury Porosimetry Measurements. The surface area of the silicalite (5 m^2/g), ZSM-5 (16 m^2/g), and LZ-105 (10 m^2/g) was determined by mercury porosimetry.[10]

Measurement of Adsorption Isotherms. The amount of oMeDBK adsorbed on the zeolite was determined by a standard depletion method.[24] A stock solution of 0.544 M oMeDBK in isooctane was employed. Solutions were diluted to predetermined concentrations with isooctane and added to 100 mg of zeolite. The amount of oMeDBK was determined by UV analysis of the supernatant at 304 nm. From

(19) Adamson, A. W. *Physical Chemistry of Surfaces*, 5th ed.; John Wiley: New York, 1990.
(20) Turro, N. J.; Weed, G. C. *J. Am. Chem. Soc*. **1983**, *105*, 186.
(21) Sokol, P. E. *Organic Syntheses*; Wiley: New York, 1973; Collect. Vol. 5, p 706
(22) Nystrom, R. F.; Brown, W. G. *J. Am. Chem. Soc*. **1947**, *69*, 2548.
(23) Ruhoff, J. R. *Organic Syntheses*; Wiley: New York, 1943; Collect. Vol. 2, p 292.
(24) Giles, C. H. M.; Mehta, H. V.; Stewart, C. E.; Subramanian, R. V. R. *J. Chem. Soc*. **1954**, 4360−4374.

the difference of the concentrations of the solution and supernatant before and after the adsorption, the amount of oMeDBK adsorbed on the zeolite was computed.

Acknowledgments. The authors at Columbia gratefully acknowledge the assistance of Dr. John Williams and Dr. Steffen Engel in upgrading the ^{2}H NMR spectrometer at Columbia University. They also thank the Kanagawa Academy of Science and Technology (KAST) and the National Science Foundation (CHE-98-12676) for generous support of this research. This work was supported in part by the National Science Foundation and the Department of Energy under Grant No. NSF CHE 9810367 to the Environmental Molecular Sciences Institute (EMSI) at Columbia University.

JA001712S